2023

Cavitation Erosion and Corrosion Resistance of Hydrophobic Sol-gel Coatings on Aluminium Alloy

Manasa Hegde
Department of Aerospace and Mechanical Engineering, South East Technological University, Carlow, Ireland

Joseph Mohan
Technological University Dublin, Joseph.Mohan@TUDublin.ie

Muhammad Qasim Mushtaq Warraich
Technological University Dublin, d15128668@mytudublin.ie

See next page for additional authors

Funder: Irish Research Council Government of Ireland Postgraduate Scholarship under Project ID GOIPG/2021/24.

Wear 524-525 (2023) 204766

Contents lists available at ScienceDirect

Wear

journal homepage: www.elsevier.com/locate/wear

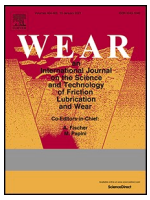

Cavitation erosion and corrosion resistance of hydrophobic sol-gel coatings on aluminium alloy

Manasa Hegde [a,b], Joseph Mohan [c], Muhammad Qasim Mushtaq Warraich [c], Yvonne Kavanagh [b], Brendan Duffy [c], Edmond F. Tobin [a,b,*]

[a] Department of Aerospace and Mechanical Engineering, South East Technological University, Carlow, Ireland
[b] The Center for Research and Enterprise in Engineering (engCORE), South East Technological University, Carlow, Ireland
[c] Centre for Research in Engineering and Surface Technology (CREST), FOCAS Institute, Technological University Dublin – City Campus, Kevin Street, Dublin D08 CKP1, Ireland

ARTICLE INFO

Keywords:
Sol-gel coating
MAPTMS
Cavitation erosion
Hydrophobicity

ABSTRACT

Cavitation erosion and erosion-corrosion are the popular failure modes of hydronautics components namely propellers, valves, turbines etc which occurs due to mechanical destructions and electrochemical corrosion. Erosion corrosion is caused due to surge in the number of solid particles affecting the surfaces whereas cavitation erosion is caused due to steady collapse of cavities or bubbles. Aluminium alloys are widely used in marine renewable industries owing to its high strength, light weight and good corrosion resistance. Despite that, cavitation and erosion-corrosion are the limiting factors for these alloys. The aim of the present work is to produce a coating system capable of replacing chromate-conversion coatings on aluminium alloy by combining an anodised layer with additional deposition of superhydrophobic sol-gel coatings. Fundamental characteristics that affect the coating's corrosion and cavitation erosion namely adhesion and thickness was evaluated. Hardness and elastic modulus of the coatings was evaluated using a Nanoscratch mechanical tester. Electrochemical behaviour of the coatings was assessed using Potentiodynamic scanning (PDS) and electrochemical impedance spectroscopy (EIS). Prolonged performance was studied using neutral salt spray test (NSS). Cavitation erosion resistance of the coatings was investigated in laboratory using a standard ultrasonic test apparatus according to ASTM G32-16. Erosion rate of the coatings was evaluated based on cumulative mass loss v/s testing time. SEM/EDX was used to evaluate the surface damage caused by erosion-corrosion and cavitation erosion. The analysis was done aiming to decide if the developed coatings was a better alternative to protect the metals from corrosion and cavitation erosion.

1. Introduction

Cavitation erosion is one of the prominent failure modes of hydronautics components namely propellers, valves, turbines etc which occurs due to mechanical destructions and electrochemical corrosion [1]. Cavitation erosion is a complex phenomenon dependent on both liquid and material properties [2], which involves the rapid formation and collapse of bubbles in a liquid due to pressure fluctuations. The essential liquid properties such as vapor pressure, bulk modulus, density, surface tension and material properties such as yield strength, tensile strength, hardness and strain influences the cavitation erosion resistance [3,4]. The bubbles collapse near the surface of the metal which results in the generation of shock waves and microjets producing pits and mass removal of the surface material, greatly affecting their efficiency and reducing their operational life [5]. Generally, maritime industries including marine vessels, ship propellers and control valves are highly affected by cavitation erosion which may further increase the material loss by the breakdown of surface passive layer [6–10]. High strength materials namely alloy of steel, cobalt-based superalloys and nickel degrade due to the aggressive nature of cavitation erosion [11–13]. High Entropy alloys (HEAs) with exceptional mechanical and corrosion resistance properties have displayed promising cavitation erosion resistance in recent times [14,15]. Despite that, they possess significant challenges for industrial applications due to higher manufacturing cost and homogenization [16–18]. Besides cavitation erosion, corrosion of aluminium and its alloys also causes huge financial losses in various

* Corresponding author. Department of Aerospace and Mechanical Engineering, South East Technological University, Carlow, Ireland.
E-mail address: edmond.tobin@setu.ie (E.F. Tobin).

https://doi.org/10.1016/j.wear.2023.204766
Received 19 September 2022; Received in revised form 2 December 2022; Accepted 4 January 2023
Available online 24 March 2023

industries and have adverse effects not merely on economy but also on human health and the environment [19,20]. Hence it is very important to protect the materials from corrosion and methods to prevent corrosion depends on the type of corrosion. Galvanic corrosion can be protected either by cathodic protection in which the anode acts as a sacrificial metal to protect a metal which becomes its cathode [21] or by using direct current from an external power source, providing sufficient current for protecting the metal [22–24]. Pitting and crevice corrosion depends on environmental parameters such as chloride concentration, temperature, and pH [25]. Aluminium and its alloys are widely used in various industries ranging from automobile to aerospace because of its properties such as lightweight, high strength, corrosion resistance etc [26]. For example, AA2024-T3 is the preferred material in aerospace industries due to its low density and productive mechanical properties [27]. In addition to this, AA2024-T3 are bound to form a stable oxide layer which protects the metal from corrosion [28]. Despite that, due to irreversible redox reactions (corrosive species attacking the metal) these metal alloys undergo corrosion when exposed to highly corrosive environment [29]. Hence, it is necessary to pre-treat the aluminium. Over the past few years, the metal alloys are protected from the damage caused by cavitation erosion using hard material coatings which are prepared from surface modifications [30] namely laser surface alloyed coatings [31] diamond-like carbon films [32], thermal spraying, anodic oxidation etc [33,34]. Regardless, it was discovered that coatings produced from thermal spraying and laser cladding was brittle and irregular [34,35] whereas, anodic oxide and diamond like carbon coatings had lower hardness and thickness which was difficult to carry a contact load [36,37]. Therefore, it is essential to prepare a coating which increases the surface performance and resist corrosion and cavitation erosion for aluminium alloys. Among, various other coating systems, sol-gel coatings have considered to be the best as it provides barrier for corrosive entities and ensures good adhesion of coatings to the metal substrate [38]. Variety of organic-inorganic hybrid sol-gel materials have been studied by the researchers for various applications [39]. These coatings integrates the properties of organic (flexibility, density etc) with inorganic (scratch resistance, durability, corrosion resistance) components [40]. A multifaceted characterisation of GPTMS-TEOS coatings on AA2024 -T3 was performed previously. Coatings were deposited by means of dip and spray deposition technique and organic and water content were varied. Salt spray exposure testing (SST) for 168 h was used to test the samples. From the results, it was observed that spray coated samples performed well with the use of about 10% organic content and high-water content and dip-coated samples performed well with higher (67%) organic content and lower water content [41]. Cullen,M et al. [42] conducted experiments for a better understanding on the effect of the structure of a hybrid sol–gels prepared using two hybrid precursors, an organosilane, 3 trimethoxysilylpropylmethacrylate, and a zirconium complex prepared form the chelation of zirconium n-propoxide and methacrylic acid on the morphology and passive anticorrosion properties of coatings deposited on AA2024-T3 aluminium surfaces. The prepared coatings were identical and the structures of the hybrid sol–gel formulations were modified by altering the concentration of the transition metal complex. Clear growth in the nanoparticle size in each system as the transition metal concentration increased was analysed using DLS analyser. Materials containing a concentration of 20 and 30% of zirconium complex proved to be more corrosion resistant [43]. The hybrid sol-gel coatings synthesized from 3- trimethoxysilylpropylmethacrylate (MAPTMS) and a zirconium complex of zirconium n propoxide (ZPO) and methacrylic acid (MAAH) towards anticorrosion potential in aerospace and automobile applications was studied previously [44]. Also, the coatings with the same precursors were altered by adding a small amount of cross-linker (HMDI) and their potential in corrosion, abrasion and cavitation erosion was studied [45,46]. In addition to this, superhydrophobic coatings are also regarded as one of the possible solution in protecting the metal alloys from corrosion and erosion as they have excellent water repellent and self-cleaning properties [47]. Thus, a small amount of PFOTES is added to the prepared coatings in the present work to increase the coatings hydrophobicity. The thickness of aluminium oxide layer can be increased through the process of anodisation. The process of anodisation is generally used in the industries to increase the corrosion resistance of the aluminium alloys [48]. Additionally, the authors [49–51] used nanoindentation technique for low ductility of Fe-based amorphous alloys to evaluate their mechanical properties. Therefore, in the present work, nanoindentation test was used to evaluate the hardness (H), Young's modulus (E) and co-efficient of friction (CoF). Since, the wear resistance depends not only on the hardness but also on the 'plasticity index', the ratios of H/E was calculated which are important to predict the service life of a component or device. Hence, in the present work, the comparison between anodised and bare coated AA2024-T3 has been investigated. Though cavitation erosion resistance properties of hydrophobic sol-gel coatings on steel and AA5083 aluminium alloy has been studied and reported [52,53], to the best of our knowledge, hardness, elastic modulus, corrosion and cavitation erosion on bare and anodised AA2024-T3 alloy has not yet been studied in detail.

Therefore, in the present work sol-gel coatings from 3- trimethoxysilylpropylmethacrylate (MAPTMS) and a zirconium complex of zirconium n propoxide (ZPO) and methacrylic acid (MAAH) with an addition of 1% of PFOTES (Perfluorooctyltriethoxysilane) hydrolysed to 25% and 50% on bare and anodised AA2024-T3 alloys were studied in detail. Uncoated bare and anodised AA2024-T3 was used as the control.

2. Materials and methods

2.1. Sol-gel synthesis

The sol-gel coatings are synthesized by the generation of stable and identical sols derived by mixing two hybrid precursors namely: an organically modified silicon pre-cursor, MAPTMS (3-methacryloxypropyltrimethoxysilane, Assay 99% in methanol, Sigma Aldrich Irl.) and an organically modified zirconium complex ZPO (zirconium (IV) n-propoxide, Assay 70% in propanol, Sigma Aldrich Irl.). MAPTMS is pre-hydrolysed with nitric acid aqueous solution and stirred for a duration of 45 min. Simultaneously, ZPO chelated by MAAH (methacrylic acid, $C_4H_6O_4$, Assay >98%, Sigma Aldrich Irl) is mixed on a stirrer for a duration of 45 min. Finally, pre-hydrolysed MAPTMS and chelated ZPO are mixed for 5 min followed by a hydrolysis using deionised water to complete hydrolysis. The developed sols (80/20) were found to be transparent which indicates that the process of hydrolysis and condensation were correctly performed. To this solution, 1 wt% of PFOTES solution which was pre-hydrolysed (25% and 50%) was added dropwise and stirred for 30 min. The final generated solution was filtered using 0.45 μm and ready to coat. A flow chart of the process is shown in Fig. 1.

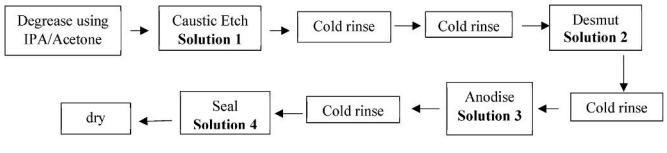

Fig. 1. Flow chart detailing the process of Anodisation.

2.2. Substrate preparation

AA2024-T3 aluminium alloy, of stated composition [54] was purchased from Impact Irl.as sheets of 1 mm thickness. In this study, AA2024-T3 alloy is pre-treated in two different ways.

Step1: Anodisation of AA2024-T3
Step 2: Pre-treatment of bare AA2024-T3

- Substrate was degreased with IPA solution.
- Substrate was then immersed in Uniclean 100 series for 1min followed by immersion in DI water for 3 min (see Table 1).

The sol-gel films on anodised and bare substrates were produced by a dip-coating technique at 100 mm/min with a holding time of 30s. Prepared films was cured at 120 °C for 2hrs in a hot air oven. Thickness of the film was 2 μm. The different types of samples used in this work are shown in Table 2.

3. Characterisation

3.1. ATR-FTIR

Fourier Transformed Infrared spectrometer with an Attenuated Total Reflectance component (ATR-FTIR, PerkinElmer Model no. 783, USA) was used to examine structural and functional groups of the prepared coating. ATR spectra were measured in a range of 4000–600 cm^{-1}.

3.2. Contact angle measurement

Wettability of the films was evaluated by measuring the contact angle (FTA surface energy analyzer) of a water droplet of 10 μl placed on the film surface using the contact angle meter equipped with a CCD camera at an ambient temperature. An average of five measurements were taken. Uncoated substrate was used as a control.

3.3. Pencil hardness test

The scratch resistance of the coatings was analysed by a pencil hardness tester (Elcometer 501) according to ASTM standard D3360-00. Pencils leads of different hardness grades (9B–9H) was used. Test was repeated at three different locations on the coatings for reliable measurements. The hardest pencil lead that does not cause damage to the coated substrate is considered as the scratch-resistant coating.

3.4. Electrochemical measurements

For potentiodynamic (PDS) and Electrochemical Impedance spectroscopy (EIS) was recorded using a Solartron SI 1287/1255B system including a frequency analyser and a potentiostat. All scans for PDS were obtained in the region from −0.5 to +1V v/s Eoc, with a scan rate of 10 mV/s at room temperatures. Experiments were performed in 3.5% NaCl solution using conventional three-electrode cell with coated samples as working electrode, saturated Ag colomel electrode as reference electrode and Pt electrode as counter electrode coupled with CorrWare software to analyse the Tafel graph. Electrochemical impedance test was performed in a frequency range from 1 × 106 to 1 × 10-1 Hz (10 points/decade) with an applied polarization amplitude of 10 mV. Impedance fitting was performed through Zview software to analyse the results.

Table 1
Chemicals and operating temperature of the anodisation process.

Solution No.	Type of solution	Composition	Operating temperature (°C)	Cycle time (min)
1	Caustic etch	1 M NaOH	55–60	2
2	Desmut	34 vol% HNO_3	Room	3
3	Anodise	15 wt% H_2SO_4	21–25	5–60
4	Seal	Water	100	5–20

Table 2
Material formulations with sample name.

Substrate	Bare AA2024-T3	Anodised AA2024-T3
Coatings reference		
No coating	Bare	Anodised
80/20 std	1 A	2 A
80/20 + 1% PFOTES (25% hydrolysed)	1B	2B
80/20 + 1% PFOTES (50% hydrolysed)	1C	2C

3.5. Neutral salt spray test (NSS)

NSS test was completed in a neutral salt spray test chamber, according to the ASTM B117 standards for 500hrs. The substrates were subjected to a salt fog environment produced from 5 wt% NaCl solution at 35 °C (±1) in an enclosed cabinet. The sides and back of the coated panel were secured with an insulating tape. The images of the substrates were taken using a digital camera after every time interval. The images were assessed to determine their corrosion potential by determining the amount of damage caused by the end of 500hrs.

3.6. Surface roughness

The Surface roughness values of the samples before corrosion and cavitation erosion tests were measured by contact probe method (Surfcom 130 A, Tokyo Seimitsu, Japan). The surface roughness of coated and uncoated samples was measured using the following parameters [55]: evaluation length of 4.0 mm, measurement speed of 0.6 mm/s and cut off value of 0.8 mm. The value of roughness was measured by taking average of three readings at different points on the plane of samples.

3.7. Cavitation erosion

Cavitation Erosion tests were completed using an ultrasonic vibratory cavitation device according to ASTM G32 standard [56]. The test was performed by using the same parameters as described in our previous paper [45]. Aluminium samples were mounted on the bottom of a transparent beaker filled with 2L of distilled water. The coating cross-section and surface damage caused by the cavitation was observed using SEM.

3.8. Nanomechanical indentation and co-efficient of friction tests

The hardness, elastic modulus and coefficient of friction measurements were conducted only on the bare and bare-coated samples using a NANOVEA CB500. The nanomechanical indentation tests were performed with a Berkovich diamond indenter having a maximum applied load of 50 mN. Loading and unloading were applied at a rate of 100 mN/min with a 10 s pause before unloading. The hardness and modulus of the bare and sol-gel coated substrates were measured and is reported as the average of 5 nanoindentation curves.

Coefficients of friction (CoF) results were taken by this device using a conical indentor with 10-μm radius. A constant load of 10 nm was used to measure the CoF over a test length of 2 mm .

4. Results and discussion

4.1. ATR-FTIR

The chemical composition of the sol-gel coatings deposited on bare and anodised aluminium substrate was investigated by the ATR-FTIR

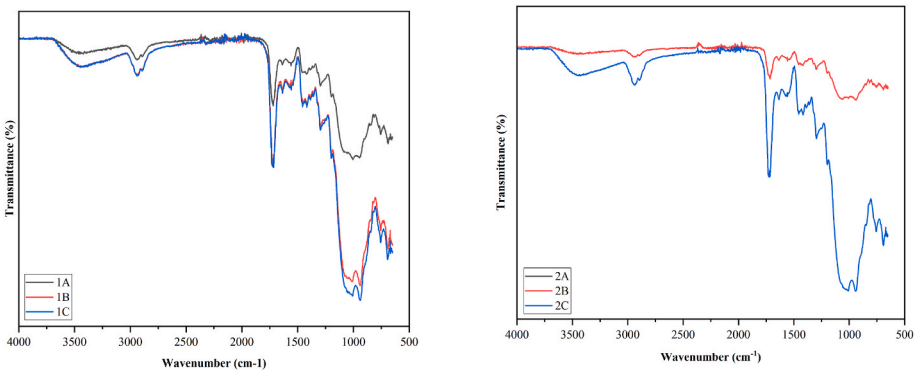

Fig. 2. ATR-FTIR spectra of (a)Bare AA2024 coated samples, (b) Anodised AA2024 coated samples.

spectroscopy. The spectra for all the coatings were obtained in the ATR mode within a spectral range of 650–4000 cm^{-1}. From, Fig. 2 it is observed that ATR-FTIR spectra for prepared coatings displayed similar chemical vibrations, as same chemicals and uniform preparation process was used, only difference being the addition of PFOTES. The band at 3400 cm^{-1} and 2840 cm^{-1} shows the presence of Si–OH and Si–OCH_3 indicating the process of hydrolysis. Bands situated in the range 800–1200 cm^{-1} indicates the presence of silicate network arising from silanol stretches Si–OH, Si–O–Si and Si–O–Zr vibrations. Si–O–Si present in methoxy-silane groups of MAPTMS is represented by the band noticed at 1170 cm^{-1}. The condensation process and the formation of silicon dioxide network is illustrated by Si–O–Si bond. Bands situated in the region 1300–1650 cm^{-1} represents Zr–OH and Zr–O–C bonds comprising the zirconium complex [57]. The Si–OH band observed in both the FT-IR spectra illustrates that surface hydroxyls remains, despite the fact the materials show the strong water repellent properties [58].

4.2. Contact angle measurements

The contact angles were measured at five different spots for each coated samples, and an average value was chosen as the contact angle. Uncoated bare and anodised samples are considered as control. The water contact angle of the coatings on bare and anodised samples are presented in Fig. 3. Uncoated bare and anodised substrate yield a contact angle of 64° and 23°, the uncoated substrates are hydrophilic in nature because polar aluminium hydroxide and oxide groups are present on the surface.

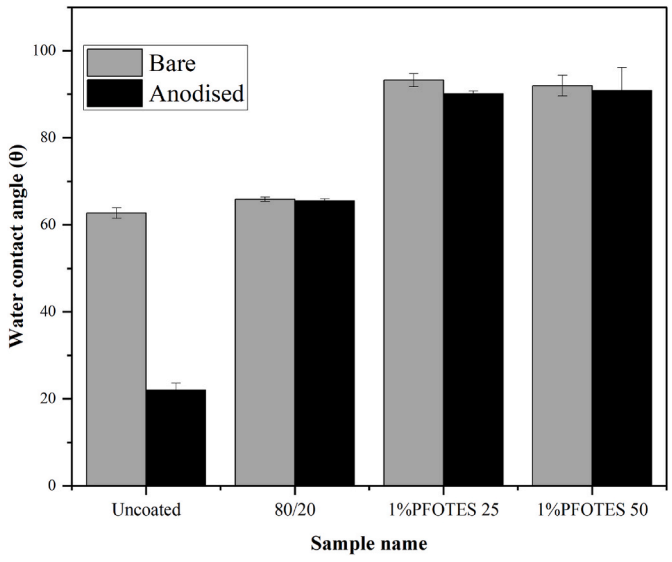

Fig. 3. Static contact angle of water droplet on sol-gel coated bare and anodised substrates.

From the results (Fig. 3), it is apparent that the contact angle of the bare and anodised substrates increases when coated with silane coatings due to the decrease in the surface roughness. It is disclosed that increase in the surface roughness results in the quick spread of water droplet on the surface [59]. The average water contact angle for 80/20 (1 A) on both bare and anodised sample is 72°, however in case of coatings with 1% PFOTES (1B and 1C) content (hydrolysed 25% and 50%) on bare coated substrate displayed a contact angle of 93° and 91° which was marginally higher than anodised coated substrate. The results exhibits that the pure sol-gel (80/20) is hydrophobic in nature due to the presence of zirconium. The coating surface has increased hydrophobicity after the addition of PFOTES.

4.3. Pencil hardness

Pencil hardness test was analysed by the level of hardness of the pencil. Test was repeated at three different locations on the coatings for reliable measurements. Coatings on both bare and anodised substrate displayed a pencil hardness of >9H. The absence of scratch was observed and confirmed visually.

4.4. Potentiodynamic polarization study (PDS)

Potentiodynamic polarization study gives practical details on electrochemical parameters like corrosion potential (Ecorr) and corrosion current densities (Icorr) [60]. Fig. 4a and b shows the results of potentiodynamic polarization curves and Table .3 gives the electrochemical parameters such as Ecorr, Icorr (which is derived from the Tafel graph) and Rp (calculated using Stern-Geary equation) [45]. The potentiodynamic curves of bare and anodised AA2024-T3 were compared with the coated bare and anodised substrates to determine the amount of reduction in corrosion current, anodic/cathodic protection and change in corrosion potential. From the results, it is evident that bare AA2024-T3 has the highest corrosion current and lowest corrosion resistance (Rp) values. Corrosion current densities in the order of 10^{-9} to $10^{-8}A/cm^2$ demonstrate the formation of strong films with good barrier properties. Corrosion resistance of 2 A is the highest compared to other coated substrates. From Table .3, coatings with addition of 1% PFOTES (25 &50% hydrolysed) on both bare and anodised substrates have displayed a good corrosion resistance which indicates that the coatings are capable of providing effective physical barrier against corrosive attacks.

4.5. Electrochemical impedance spectroscopy

The impedance data for the prepared coatings on both bare and anodised substrates after initial exposure to the electrolyte solution is shown in Fig. 5. The coatings resistance to the AC signal, or impedance differs based on the applied frequency and is presented graphically by a

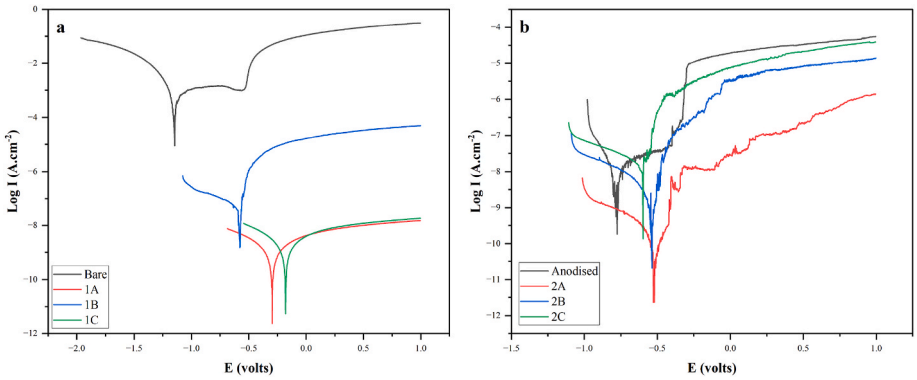

Fig. 4. Potentiodynamic curves of sol-gel coatings on (a) Bare samples, (b) Anodised samples.

Table 3
Corrosion parameters determined from potentiodynamic scan of bare, anodise and sol-gel coated samples on bare and anodised AA2024-T3.

Sample name	-Ecorr (V)	Icorr (Acm^{-2})	Rp (cm^2)
Bare	−0.661	3.52×10^{-7}	3.9×10^{2}
Anodised	−0.776	5.9×10^{-9}	4.97×10^{6}
1 A	−0.295	1.35×10^{-9}	6.8×10^{7}
1B	−0.579	4.8×10^{-8}	1.3×10^{7}
1C	−0.179	2.17×10^{-9}	4.38×10^{7}
2 A	−0.523	1.79×10^{-10}	3.15×10^{8}
2B	−0.529	2.07×10^{-9}	1.08×10^{7}
2C	−0.598	1.90×10^{-8}	1.63×10^{6}

bode plot which contributes a good comparison of total impedance values for coated and uncoated samples. it is clear from the graph, that the coated bare and anodised samples display a lower corrosion rate compared to uncoated bare and anodised substrate.

Fig. 5 (a and b) shows bode plots for bare, anodised and sol-gel coatings. The impedance of bare AA2024-T3 is in the range of 10^4 Ω at low frequencies, in contrast the impedance value of uncoated anodised layer is increased to the range of 10^{10}Ω in the same frequency range. Coating the bare samples with sol-gel layers has increased the impedance by at least three-four orders of magnitude. The anodised layers with sol-gels however have shown one order decrease in the magnitude of impedance value compared to the uncoated anodised sample. The impedance of 1B,1C,2B, 2C increases to 10^8Ω. Therefore, it is evident that the prepared sol-gels acted as an effective barrier against corrosive electrolyte influx during EIS measurements. Addition of 1% of PFOTES (25% and 50% hydrolysed) provided a better barrier with higher impedance values.

Film properties including barrier performance and interfacial activity are provided by phase angle with impedance data (Fig. 5 c, d). The data signifies that both bare and anodised coated samples had a phase angle of ~20° at 10^{-1} Hz and maintains a phase angle of ~80° near the mid-frequency range which indicates higher corrosion barrier properties [61].

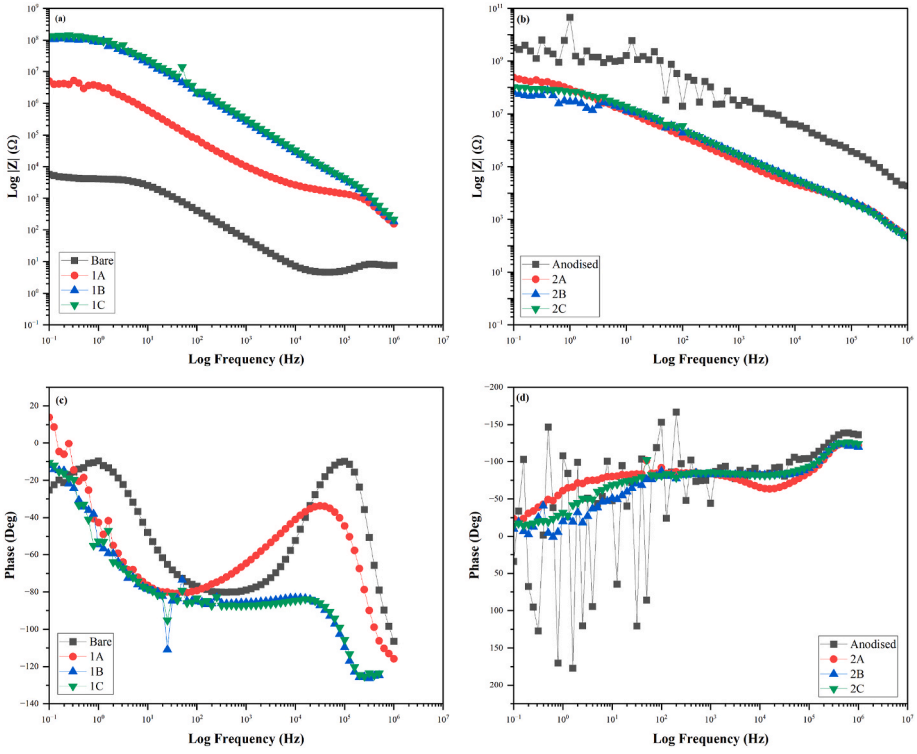

Fig. 5. EIS spectra representing (a) Bode plots of bare and coated AA2024-T3, (b)Bode plots of anodised and coated AA2024-T3, (c) Phase diagrams for bare and coated AA2024-T3, (d) Phase diagrams for anodised and coated AA2024-T3.

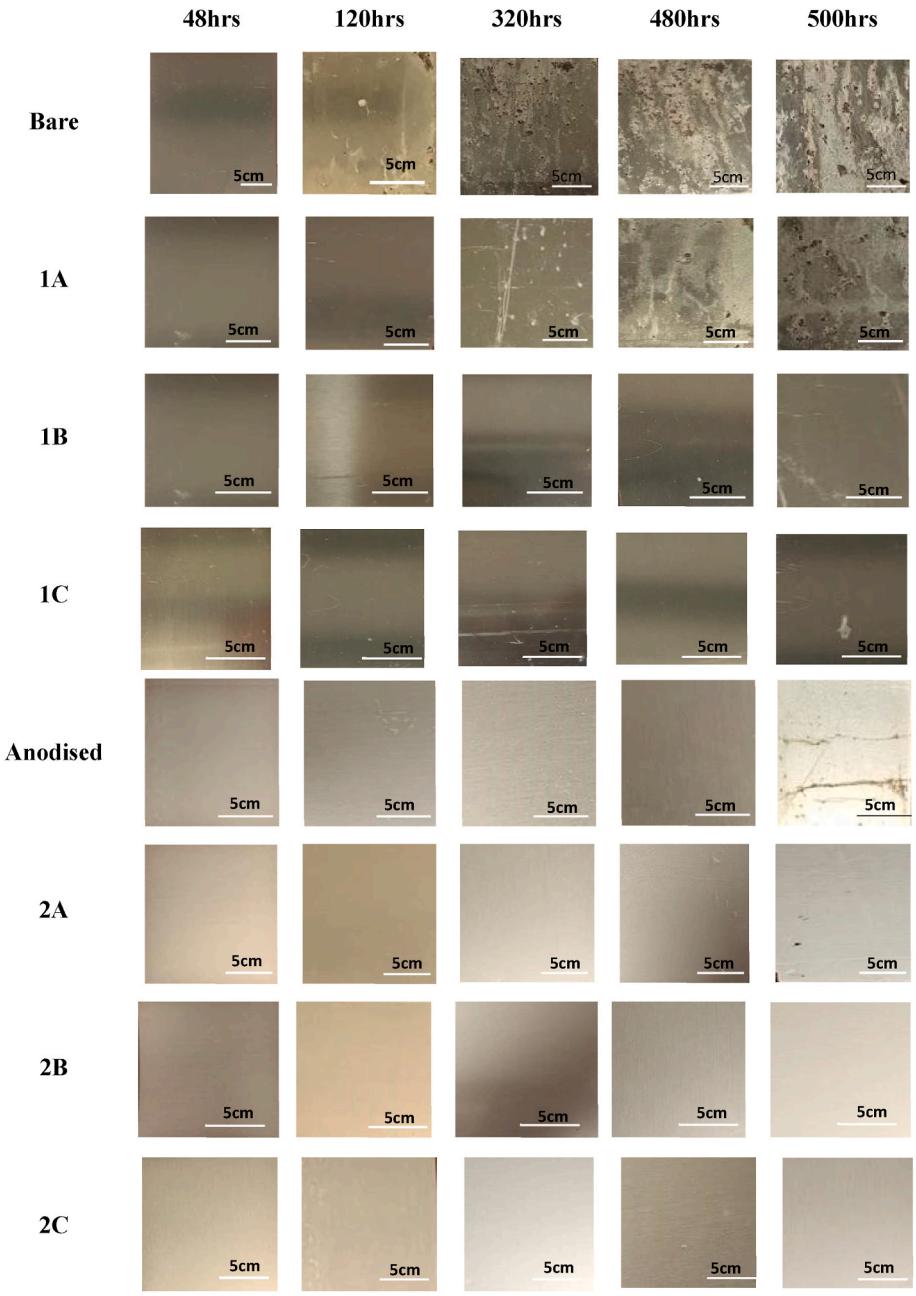

Fig. 6. Photographs of uncoated and coated samples after 500hrs exposure in a salt-spray chamber.

4.6. Neutral salt spray test

The neutral salt spray test was used to determine the corrosion resistance performance of bare, anodised and sol-gel coated samples. The test was conducted for 500hrs. The results from the test for the samples are shown in Fig. 6. The coatings was said to be failed if three or more pits were observed per panel [62]. Bare and anodised AA2024-T3 was used as the reference. The bare alloy displayed minimal resistance to corrosion in the neutral salt spray test as it reported corrosion after 120hrs. Anodised alloy however survived the salt spray test until the end of 480 h, damage on the substrate with pits was observed by the end of 480hrs.

The pit formation on 80/20 (1 A) coating on bare AA2024-T3 started between 320 and 480hrs, with substantial corrosion product formation by the end of 500hrs. However, there was no damage on the 80/20 (2 A) coating on anodised alloy till the end of 500hrs.

Anodised panels coated with 80/20 + 1%PFOTES (25% and 50% hydrolysed) provided a good active corrosion protection as no significant accumulation of corrosion products on the panels were detected even after the exposure to salt spray for 500hrs.

4.7. Surface roughness

Surface roughness measurements were performed with a stylus profilometer to evaluate any fundamental variations and changes in the surface roughness of bare, anodised and coated AA2024-T3. Number of roughness parameters can be used to measure the roughness of a surface. In the present work, arithmetic mean roughness (Ra) was measured. The surface roughness of the substrates used in this study are displayed in Table 4. All coated specimens displayed even surfaces with Ra less that 0.1 μm. Significant increase in the surface roughness of uncoated anodised substrate was observed due to the combined anodising conditions

Table 4
Average surface roughness of bare/bare coated and anodised/anodised coated samples.

Sample name	Ra (μm)
Bare uncoated	0.157
Anodised uncoated	0.429
1 A	0.054
1B	0.051
1C	0.035
2 A	0.061
2B	0.082
2C	0.051

and method used to anodise the substrates. It was observed an increase in WCA may be due to the increase in surface roughness (Fig. 3 and Table 4). However, due to low predominance of the roughness variations, the measurements of the hardness, elasticity, CoF correlated properties were not affected by the roughness.

4.8. Cavitation erosion

The cavitation erosion cumulative mass loss curves from 0 to 42 min for bare, anodised and coated samples are shown in Fig. 7. The thickness of the coatings was ~2 μm; hence cavitation erosion tests were performed for a short period of time. There is significant difference in the mass loss between bare and anodised coated samples. All of the coated samples displayed a mass loss lower than uncoated AA2024-T3. Along, with the mass loss, we also observed the time at which the coating was delaminated from the substrate. In our previous work [45], we reported that the coatings prepared from the same precursors survived cavitation erosion up to 7 min, whereas from the results indicated in the present work, it was observed that 1 A and 2 A could resist cavitation erosion up to 30 min. The coatings 1B and 1C could resist cavitation erosion resistance up to 12 min, whereas the coatings 2B and 2C could withstand cavitation erosion up to 20 min. This indicated that the 1 A and 2 A coatings could greatly increase the cavitation erosion resistance.

Surface morphology of the uncoated and coated samples after the end of 42 min of cavitation test was observed through SEM to observe the number of cavitation pits formed on the surface of the substrate. Fig. 8, reported different appearances for each sample. Uncoated bare and anodised substrates were attacked, and numerous cavitation pits were created on the substrate, which therefore resulted in higher mass loss for these samples. Contrastingly, the coatings on the bare substrate (1 A, 1B and 1C) exhibited regular plastic deformation traces with no visible pits (Fig. 8a, b, c). In 1B and 1C coatings, no erosion damage was developed after 42 min of the test with no detectable pits (Fig. 8b and c). Likewise, the surface with 1 A coating did not display pitting, such as that of bare and anodised uncoated substrate, despite that small cavities are observed from the loss of small pieces of material being eroded (Fig. 8a).

A variety of patterns could be seen on the surface of the anodised coatings 2 A, 2B and 2C (Fig. 8d, e, f) caused due to fatigue mechanism and plastic deformation. Small island observed in Fig. 8d and f, which indicates the presence of microcracking to a lesser degree. For the 2B coating, the eroded surfaces seem to be a little different. SEM analysis indicated that this coating fragmented quickly due to cavitation pulses striking the surface that has resulted in the formation of craters and small pits that are less than 1 μm in diameter (Fig. 8e). Porosity of both bare and anodised coated samples were analysed using ImageJ software (taking cross-section areas of the samples from SEM images). There was a strong correlation observed between porosity and corrosion-erosion results (Table 5). Bare/bare coated samples displayed a higher % porosity whereas, the anodised/anodised coated samples displayed a lower porosity. The higher porosity sample had low corrosive and erosive resistance compared to the samples showing low porosity.

4.9. Nanomechanical indentation & coefficient of friction tests

The indentation data for only bare and coated AA2024-T3 was reported in this work. Anodised samples were not considered for the indentation test. Table 6 lists the hardness and modulus values of the bare and coated samples. From the results it was observed that, 1C was about 25% less than 1 A. However, 1B coating displayed a higher hardness compared to 1 A and 1C. As expected, there was a positive correlation between modulus and hardness [63].

From Fig. 9a, it was evident that the samples are indented steadily and the maximum applied load (i.e 50 nm) is reached at a lower depth for the bare substrate as opposed to each sol-gel coated sample (see Table 6). 1B coating showed highest hardness and modulus. The hydrophobic nature of PFOTES may have increased the volume of these pores which, due to the hardness and the elasticity may have reduced when compared to the bare substrate. Fig. 9b shows CoF results for bare and coated samples. It was observed that, the CoF values of the bare substrate was higher than the coated substrates. From the graph (Fig. 9b), fluctuations are observed for all the samples, this represents the path at which the scratch tip enters and leaves the surface of the sample. While the difference is not notable in the absolute value of the CoF of bare versus either of the three sol-gel coated samples, it was noted

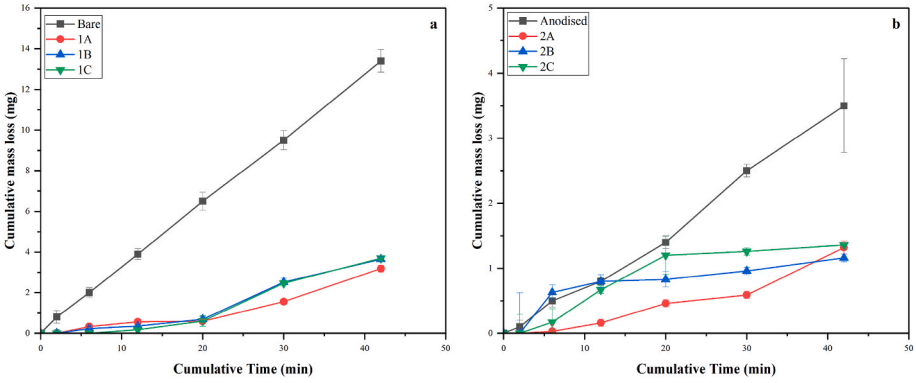

Fig. 7. Graphical illustration of cumulative mass loss during cavitation test for (a) bare and coated AA2024-T3, (b) anodised and coated AA2024-T3.

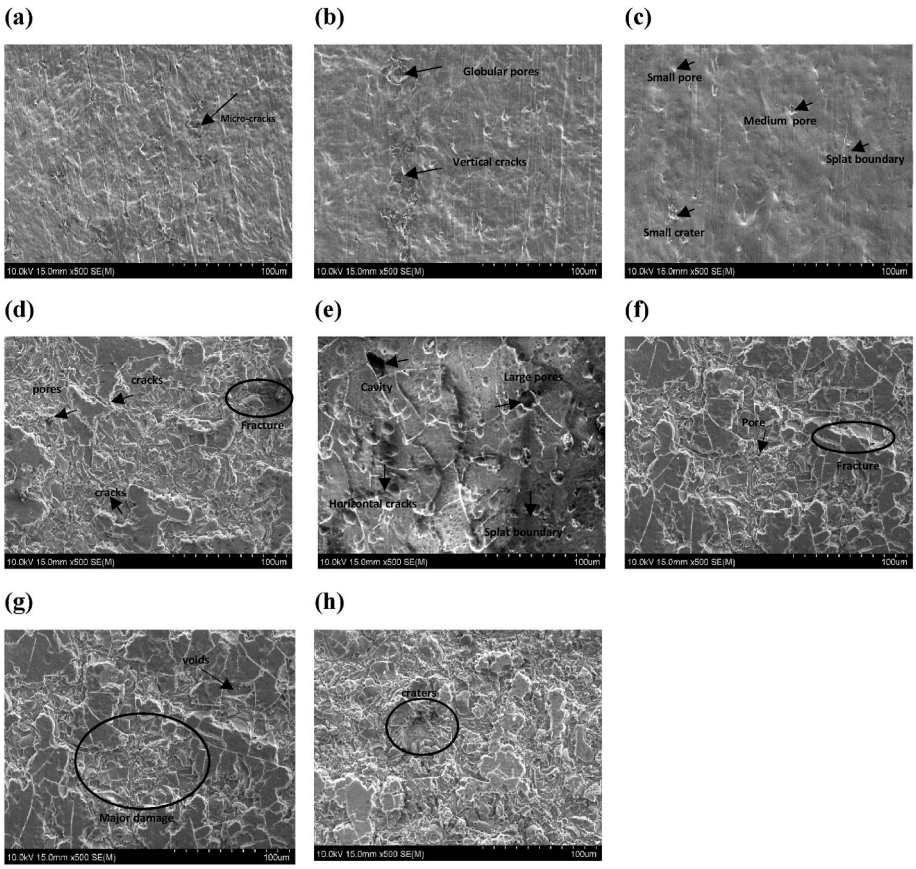

Fig. 8. SEM images of (a)1 A, (b) 1B, (c)1C, (d)2 A, (e)2B, (f)2C, (g)Bare AA2024-T3, (h)Anodised AA2024-T3.

Table 5
Porosity values determined for the samples after cavitation erosion test.

Sample	% Porosity	Average Particle Size
Bare AA2024-T3	17.94	14.71
Anodised AA2024-T3	8.12	14.47
1 A	7.04	14.17
1B	15.05	13.84
1C	10.74	11.23
2 A	6.15	14.31
2B	0.68	8.813
2C	4.23	3.081

Table 6
Hardness and modulus of different coatings on bare AA2024.

Sample	Depth (nm)	Load (mN)	Hardness (GPa)	Youngs Modulus	CoF
Bare	1.07	49.71	2.14	55.0	1.89
1 A	2.70	49.76	0.42	5.4	1.68
1B	2.64	49.64	0.42	5.8	1.73
1C	2.83	49.78	0.41	4.4	1.96

that the traces for the bare samples were 'noisier' than the coated samples (see Fig. 9 (b)). This may indicate that there was more 'stick-slip' type movement of the conical indentor over the sample compared to the relatively 'smoother' coated samples.

Furthermore, the ratio of hardness and elastic modulus (H/E) used as an index to predict the cavitation erosion was evaluated. Hardness (H) and elastic modulus (E) values for coated and uncoated aluminium was extracted from the indentation results. The ratio between H and E values for bare substrate was 3.7 GPa and increased significantly for coated samples from 6.1, 7.3 and8.1 GPa for 1 A, 1B and 1C, respectively. The higher H/E value, the higher the cavitation erosion resistance of the coating. In addition to this, substrate with a larger H/E value indicates that it will experience a larger elastic strain before failure caused by subsequent plastic deformation and fracture, and thus it has a higher capability to resist contact pressures when subjected to cavitation damage.

5. Conclusions

The objective of this research was to identify the effect PFOTES (25% and 50% hydrolysed) had on the hardness, wetting, corrosion and cavitation erosion when coated on bare and anodised AA2024-T3. Coatings were structurally analysed by ATR-FTIR and the wetting properties were determined by WCA measurements. FT-IR analysis displayed the formation of siloxane and Si–O–Zr bonds within the network. The wettability analysis exhibited that uncoated bare and anodised AA2024-T3 displayed very low contact angle whereas the CA for 80/20 on both bare and anodised sample was 72°, and in coatings with 1% PFOTES (hydrolysed 25% and 50%) on bare coated substrate displayed a contact angle of 93° and 91° which was marginally higher than anodised coated substrate. Scratch resistance properties of the coatings analysed through PHT indicated that all the coatings on both bare and the anodised samples had a hardness of >9H. PDS, EIS and NSS results confirmed that the addition of PFOTES into sol–gel increased the corrosion protection ability of coating. Surface morphology from the cavitation test indicated that plastic deformation was caused by the implosion of bubbles which resulted in the increase of cavities and micro-cracks in anodised coated samples (with and without PFOTES) compared to the coatings on bare substrate. The tribological tests revealed that the bare substrate had higher hardness and modulus values compared to the coated substrates. However, CoF was low in 1 A and 1B

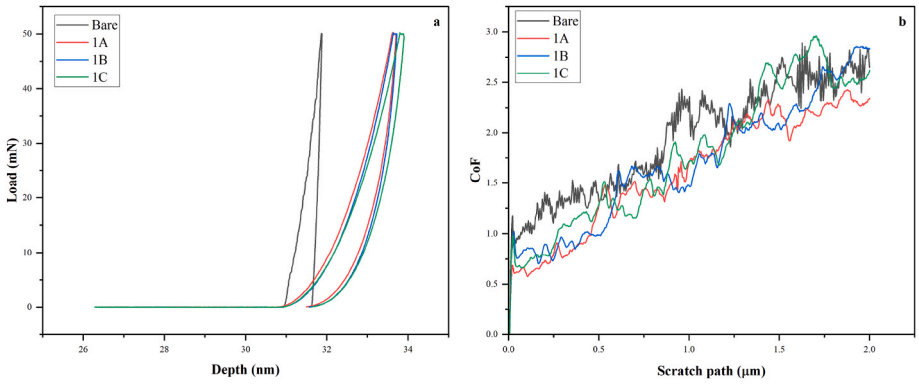

Fig. 9. (a) Load-depth curves for bare and coated AA2024-T3, (b) Coefficient of friction (CoF) curves for bare and coated AA2024-T3.

coatings on bare substrate which indicated the best wear behaviour.

To put it concisely, the measured addition of PFOTES to the developed sol-gels (80/20) creates a promising path to create a highly organic-inorganic network which produces thin coatings with excellent corrosion and erosion resistance properties as applied on bare and anodised AA2024-T3 alloys. However, further work needs to be completed to investigate the relationship between roughness, hardness, elasticity and plasticity of bare anodised and coated anodised samples.

Statement of originality

Statement of originalityThe research work described in this paper is, to the best of our knowledge and belief, original, except as referenced and acknowledged in the text. The work has not been submitted elsewhere, either in whole or in part, for publication

Declaration of competing interest

The authors declare that they have no known competing financial interests or personal relationships that could have appeared to influence the work reported in this paper.

Acknowledgements

The research is funded by the Irish Research Council Government of Ireland Postgraduate Scholarship under Project ID GOIPG/2021/24.

References

[1] J. Chang, et al., Cavitation erosion and corrosion behavior of Ni–Al intermetallic coatings, Wear 255 (1–6) (2003) 162–169.
[2] B. Sreedhar, S.a. Albert, A. Pandit, Improving cavitation erosion resistance of austenitic stainless steel in liquid sodium by hardfacing–comparison of Ni and Co based deposits, Wear 342 (2015) 92–99.
[3] A. Thiruvengadam, A Unified Theory of Cavitation Damage, 1963.
[4] R. Garcia, F.G. Hammitt, Cavitation Damage and Correlations with Material and Fluid Properties, 1967.
[5] C. Lin, K. Chen, J. He, The cavitation erosion behavior of electroless Ni–P–SiC composite coating, Wear 261 (11–12) (2006) 1390–1396.
[6] K. Selvam, et al., Exceptional cavitation erosion-corrosion behavior of dual-phase bimodal structure in austenitic stainless steel, Tribol. Int. 134 (2019) 77–86.
[7] J. Basumatary, R. Wood, Synergistic effects of cavitation erosion and corrosion for nickel aluminium bronze with oxide film in 3.5% NaCl solution, Wear 376 (2017) 1286–1297.
[8] J. Ryl, K. Darowicki, P. Slepski, Evaluation of cavitation erosion–corrosion degradation of mild steel by means of dynamic impedance spectroscopy in galvanostatic mode, Corrosion Sci. 53 (5) (2011) 1873–1879.
[9] G. Bregliozzi, et al., Cavitation wear behaviour of austenitic stainless steels with different grain sizes, Wear 258 (1–4) (2005) 503–510.
[10] A. Al-Hashem, et al., Cavitation corrosion behavior of cast nickel-aluminum bronze in seawater, Corrosion 51 (5) (1995).
[11] M. Yao, et al., A novel, single phase, non-equiatomic FeMnNiCoCr high-entropy alloy with exceptional phase stability and tensile ductility, Scripta Mater. 72 (73) (2014) 5–8.
[12] K.C. Antony, Wear-resistant cobalt-base alloys, JOM 35 (2) (1983) 52–60.
[13] C. Kwok, H.C. Man, L. Leung, Effect of temperature, pH and sulphide on the cavitation erosion behaviour of super duplex stainless steel, Wear 211 (1) (1997) 84–93.
[14] R.B. Nair, H. Arora, H. Grewal, Microwave synthesized complex concentrated alloy coatings: plausible solution to cavitation induced erosion-corrosion, Ultrason. Sonochem. 50 (2019) 114–125.
[15] R. Nair, et al., Exceptionally high cavitation erosion and corrosion resistance of a high entropy alloy, Ultrason. Sonochem. 41 (2018) 252–260.
[16] R.J. Wood, Erosion–corrosion interactions and their effect on marine and offshore materials, Wear 261 (9) (2006) 1012–1023.
[17] C. Wu, et al., Phase evolution and cavitation erosion-corrosion behavior of FeCoCrAlNiTix high entropy alloy coatings on 304 stainless steel by laser surface alloying, J. Alloys Compd. 698 (2017) 761–770.
[18] Y. Zhang, X. Yang, P. Liaw, Alloy design and properties optimization of high-entropy alloys, JOM (J. Occup. Med.) 64 (7) (2012) 830–838.
[19] N. Dimitrov, J. Mann, K. Sieradzki, Copper redistribution during corrosion of aluminum alloys, J. Electrochem. Soc. 146 (1) (1999) 98.
[20] P.A. Sørensen, et al., Anticorrosive coatings: a review, J. Coating Technol. Res. 6 (2) (2009) 135–176.
[21] M. Kendig, D.J. Mills, An historical perspective on the corrosion protection by paints, Prog. Org. Coating 102 (2017) 53–59.
[22] M.H.A. Bakar, et al., Can electrochemically active biofilm protect stainless steel used as electrodes in bioelectrochemical systems in a similar way as galvanic corrosion protection? Int. J. Hydrogen Energy 44 (58) (2019) 30512–30523.
[23] B. Illes, et al., Corrosion-induced tin whisker growth in electronic devices: a review, Solder. Surf. Mt. Technol. 29 (1) (2017) 59–68.
[24] D.N. Dang, et al., Influence of soil moisture on the residual corrosion rates of buried carbon steel structures under cathodic protection, Electrochim. Acta 176 (2015) 1410–1419.
[25] H.S. Klapper, et al., Environmental factors affecting pitting corrosion of type 304 stainless steel investigated by electrochemical noise measurements under potentiostatic control, Corrosion Sci. 75 (2013) 239–247.
[26] W. Miller, et al., Recent development in aluminium alloys for the automotive industry, Mater. Sci. Eng., A 280 (1) (2000) 37–49.
[27] K. Emregül, A.A. Aksüt, The behavior of aluminum in alkaline media, Corrosion Sci. 42 (12) (2000) 2051–2067.
[28] E. Abd, et al., Strengthening mechanisms, deformation behavior, and anisotropic mechanical properties of Al-Li alloys: a review [J], J. Adv. Res. 10 (2018) 49–67.
[29] E. Ghali, Corrosion Resistance of Aluminum and Magnesium Alloys: Understanding, Performance, and Testing, John Wiley & Sons, 2010.
[30] F. Cheng, S. Jiang, J. Liang, Cavitation erosion resistance of microarc oxidation coating on aluminium alloy, Appl. Surf. Sci. 280 (2013) 287–296.
[31] W. Tomlinson, A. Bransden, Cavitation erosion of laser surface alloyed coatings on Al-12% Si, Wear 185 (1–2) (1995) 59–65.
[32] L. Gerke, et al., Cavitation erosion resistance of aC: H coatings produced by PECVD on stainless steel and NiTi substrates, Surf. Coating. Technol. 204 (21–22) (2010) 3418–3424.
[33] Q. Liu, S.Z. El Abedin, F. Endres, Electroplating of mild steel by aluminium in a first generation ionic liquid: a green alternative to commercial Al-plating in organic solvents, Surf. Coating. Technol. 201 (3–4) (2006) 1352–1356.
[34] S. Bourban, et al., Laser cladding of Al2O3-ZrO2 eutectic on steel, Zeitschrift für Metallkunde 90 (8) (1999) 608–614.
[35] J. Cheng, et al., Synthesis and erosion behaviors of nanoscale coatings prepared by wire arc spraying, Rare Met. Mater. Eng. 41 (2012) 144–147.
[36] H.-H. Shih, S.-L. Tzou, Study of anodic oxidation of aluminum in mixed acid using a pulsed current, Surf. Coating. Technol. 124 (2–3) (2000) 278–285.
[37] A. Voevodin, S. Walck, J. Zabinski, Architecture of multilayer nanocomposite coatings with super-hard diamond-like carbon layers for wear protection at high contact loads, Wear 203 (1997) 516–527.
[38] S. Lamaka, et al., Novel hybrid sol–gel coatings for corrosion protection of AZ31B magnesium alloy, Electrochim. Acta 53 (14) (2008) 4773–4783.
[39] E. MacHugh, et al., The effect of curing and zirconium content on the wettability and structure of a silicate hybrid sol-gel material, J. Non-Cryst. Solids 525 (2019), 119658.
[40] Y. Castro, E. Özmen, A. Durán, Integrated self-healing coating system for outstanding corrosion protection of AA2024, Surf. Coating. Technol. 387 (2020), 125521.
[41] T.L. Metroke, O. Kachurina, E.T. Knobbe, Spectroscopic and corrosion resistance characterization of GLYMO–TEOS Ormosil coatings for aluminum alloy corrosion inhibition, Prog. Org. Coating 44 (4) (2002) 295–305.

[42] M. Cullen, et al., The role of the hydrolysis and zirconium concentration on the structure and anticorrosion performances of a hybrid silicate sol-gel coating, J. Sol. Gel Sci. Technol. 86 (3) (2018) 553–567.
[43] L. Delattre, C. Dupuy, F. Babonneau, Characterization of the hydrolysis and polymerization processes of methacryloxypropyltrimethoxysilane, J. Sol. Gel Sci. Technol. 2 (1) (1994) 185–188.
[44] M. Cullen, et al., Correlation between the structure and the anticorrosion barrier properties of hybrid sol–gel coatings: application to the protection of AA2024-T3 alloys, J. Sol. Gel Sci. Technol. 82 (3) (2017) 801–816.
[45] M. Hegde, et al., Multifunctional hybrid sol-gel coatings for marine renewable energy applications: synthesis, characterization and comparative analysis with organically modified silicon precursor coatings, MRS Adv. 5 (33–34) (2020) 1757–1764.
[46] M. Hegde, et al., Preliminary Evaluation of functional coatings for marine based renewable energy applications, in: Proceedings of the 13th International Conference on Damage Assessment of Structures, Springer, 2020.
[47] J.-D. Brassard, D. Sarkar, aJ. Perron, Fluorine Based Superhydrophobic Coatings, vol. 2, applied sciences, 2012, pp. 453–464.
[48] M. Whelan, et al., Corrosion inhibitors for anodised aluminium, Surf. Coating. Technol. 227 (2013) 75–83.
[49] S. Hong, et al., Hydro-abrasive erosion and cavitation-silt erosion characteristics of HVOF sprayed WC-Ni cermet coatings under different flow velocities and sand concentrations, Ceram. Int. 49 1 (2022) 74–83.
[50] J. Cheng, X. Liang, B. Xu, Devitrification of arc-sprayed FeBSiNb amorphous coatings: effects on wear resistance and mechanical behavior, Surf. Coating. Technol. 235 (2013) 720–726.
[51] S. Hong, et al., Hydro-abrasive erosion behaviors of HVOF sprayed carbide-based cermet coatings in simulated seawater slurries, Tribol. Int. 177 (2023), 108001.
[52] J. Fahim, et al., Cavitation erosion behavior of super-hydrophobic coatings on Al5083 marine aluminum alloy, Wear 424 (2019) 122–132.
[53] A.M. Emelyanenko, et al., Nanosecond laser micro-and nanotexturing for the design of a superhydrophobic coating robust against long-term contact with water, cavitation, and abrasion, Appl. Surf. Sci. 332 (2015) 513–517.
[54] M. Schem, et al., CeO2-filled sol–gel coatings for corrosion protection of AA2024-T3 aluminium alloy, Corrosion Sci. 51 (10) (2009) 2304–2315.
[55] S. Kaur, S. Sharma, N. Bala, A comparative study of corrosion resistance of biocompatible coating on titanium alloy and stainless steel, Mater. Chem. Phys. 238 (2019), 121923.
[56] G32-16, A., Standard Test Method for Cavitation Erosion Using Vibratory Apparatus, Annual book of ASTM standards, ASTM, West Conshohochen, PA, 2016.
[57] M. Cullen, et al., An investigation into the role of the acid catalyst on the structure and anticorrosion properties of hybrid sol-gel coatings, Thin Solid Films 729 (2021), 138703.
[58] A.V. Rao, et al., Mechanically stable and corrosion resistant superhydrophobic sol–gel coatings on copper substrate, Appl. Surf. Sci. 257 (13) (2011) 5772–5776.
[59] B. Ramezanzadeh, et al., Corrosion protection of steel with zinc phosphate conversion coating and post-treatment by hybrid organic-inorganic sol-gel based silane film, J. Electrochem. Soc. 164 (6) (2017) C224.
[60] M. Kendig, et al., Role of hexavalent chromium in the inhibition of corrosion of aluminum alloys, Surf. Coating. Technol. 140 (1) (2001) 58–66.
[61] P. Agilan, K. Saranya, N. Rajendran, Bio-inspired polydopamine incorporated titania nanotube arrays for biomedical applications, Colloids Surf. A Physicochem. Eng. Asp. 629 (2021), 127489.
[62] P.R. Varma, et al., Application of niobium enriched ormosils as thermally stable coatings for aerospace aluminium alloys, Surf. Coating. Technol. 205 (16) (2011) 3992–3998.
[63] O. Çomaklı, T. Yetim, A. Çelik, The effect of calcination temperatures on wear properties of TiO2 coated CP-Ti, Surf. Coating. Technol. 246 (2014) 34–39.